# Epigenetic induction of epithelial to mesenchymal transition by *LCN2* mediates metastasis and tumorigenesis, which is abrogated by NF-κB inhibitor BRM270 in a xenograft model of lung adenocarcinoma

RAJ KUMAR MONGRE[1], SIMRINDER SINGH SODHI[2], NEELESH SHARMA[3], MRINMOY GHOSH[1], JEONG HYUN KIM[1], NAMEUN KIM[1], YANG HO PARK[4], YOUNG GYU SHIN[4], SUNG JIN KIM[5], ZHANG JIAO JIAO[1], DO LUONG HUYNH[1] and DONG KEE JEONG[1]

[1]Laboratory of Animal Genetic Engineering and Stem Cell Biology, Department of Animal Biotechnology, Faculty of Biotechnology, Jeju National University, Jeju, Republic of Korea; [2]Department of Veterinary and Animal Husbandry Extension Education, Guru Angad Dev Veterinary and Animal Sciences University, Ludhiana, Punjab; [3]Division of Veterinary Medicine, Faculty of Veterinary Science and Animal Husbandry, Sher-e-Kashmir University of Agricultural Sciences and Technology, R.S. Pura, Jammu, India; [4]BRM Institute; [5]CHA Cancer Institute, CHA University, Seoul, Republic of Korea

Received September 19, 2015; Accepted October 20, 2015

DOI: 10.3892/ijo.2015.3245

**Abstract.** Tumor initiating cancer stem-like cells (TICSCs) have recently become the object of intensive study. Human-Lipocalin-2 (h*LCN2*) acts as a biomarker for cancers. The aim of the present study was to explore new insights regarding the potential role of *LCN2* in inducing epithelial to mesenchymal transition (EMT) by transfecting *LCN2* into CD133$^+$-A549-TICSCs and its cross-talk with the NF-κB signaling pathway in adenocarcinoma of the lung. Furthermore, EMT was confirmed by transcriptomic analysis, immunoblotting and immunocyto/histochemical analyses. Tumorigenesis and metastasis were confirmed by molecular therapeutics tracer 2DG infrared optical probe in BALB/cSIc-nude mice. It was observed that the CD133$^+$-expressing-*LCN2*-A549 TICSCs population increased in adenocarcinoma of the lung compared to the normal lung tissue. The expressions of genes involved in stemness, adhesion, motility and drug efflux was higher in these cells than in their non-*LCN2* expressing counterparts. The present study revealed that elevated expression of *LCN2* significantly induced metastasis via EMT. Overexpression of *LCN2* significantly increased stemness and tumor metastasis by modulating NF-κB cellular signaling. BRM270, a novel inhibitor of NF-κB plays a significant role in the EMT reversal. BRM270, a naturaceutical induces cell shrinkage, karyorrhexis and programmed cell death (PCD) which were observed by Hoechst 33342 staining while flow cytometry analysis showed significant (P<0.05) decrease in cell population from G0-G1 phases. Also, 2DG guided *in vivo* model revealed that BRRM270 significantly (P<0.0003) reduced tumor metastasis and increased percent survival in real-time with complete resection. An elaborate study on the novel concept with respect to linking of naturaceutics as selective and potential anticancer agent that eliminates the elevated *LCN2* induced EMT and tumor dissemination through cooperation with the NF-κB signaling as the baseline data for the planning of new therapeutic strategies was conducted for the first time. Our results also illustrate a molecular mechanistic approach for 2DG-guided molecular imaging-based cancer therapy using BRM270 as a novel cancer therapeutic drug to enhance the effect of doxorubicin (Dox)-resistant *LCN2* induced metastasis of solid tumors in nude mice.

*Correspondence to:* Professor Dong Kee Jeong, Department of Animal Biotechnology, Faculty of Biotechnology, Jeju National University, Ara-1 Dong, Jeju-city, Jeju-Do 690-756, Republic of Korea
E-mail: dkjeong@jejunu.ac.kr

*Abbreviations:* EMT, epithelial to mesenchymal transition; PCD, programmed cell death; FACS, fluorescence activated cell sorting; TICSCs, tumor initiating stem-like cancer cells; ANOVA, analysis of variance; NF-κB, nuclear factor kappa B; MMP-9, matrix metalloproteinase-9; *LCN2*, human Lipocalin-2; hBMCs, human bone marrow cells; 2DG, 2-deoxy-D-glucose; MDR, multiple drug resistance

*Key words:* naturaceutics, 2DG optical probe, tumor initiating cancer stem-like cells, karyorrhexis, Lipocalin-2, epithelial to mesenchymal transition

## Introduction

Stem cell research is a promising arena for the therapeutic advancement in oncology, clinical-genetics and degenerative

disorders (1-3). Focus of cancer research is on the properties and mechanisms of formation of cancer stem cells (CSCs) or tumor initiating cancer stem-like cells (TICSCs) (1,2). However, the mechanisms governing the conversion of malignant cells into CSCs are poorly understood for majority of cancers (3,4). Most soft and solid neoplasms contain specific TICSCs expressing cell surface glycoprotein markers that are different from normal cells (5,6). These putative surface markers have enabled the identification and characterization of TICSCs. Furthermore, TICSCs exist distinctly in epithelial-mesenchymal-transition (EMT) and mesenchymal-epithelial-transition (MET) states (7). Notably, EMT-induced TICSCs are efficient in inducing tumor formation and metastasis (8). $CD133^+$ (transmembrane glycoprotein cell surface marker)-TICSCs have shown phenotypical reversion from the epithelial to mesenchymal state in lung cancer stem cells (5,6).

Activation of EMT in carcinogenic cells gives rise to cells that are stem-like in nature (7,8). The EMT plays an important role in embryogenic differentiation and biological processes associated with cancer progression (6-8). During EMT, the expression of epithelial maintaining genes (E-cadherin and TJP-1) is reported to be antagonized and mesenchymal candidate marker genes (vimentin, Twist-1 and SNAI2) are augmented (9,10). During oncogenesis, EMT is associated with several signaling cascades including the NF-κB pathway (8). Overexpression of p65 (NF-κB) induces transcriptional upregulation of Twist-1 along with EMT in mammary epithelial cells.

Human Lipocalin-2 (*LCN2*) is a biomarker for many inflammatory-based diseases and cancers including lung carcinoma (11-13). Furthermore, *LCN2* has been reported to promote resistance to drug-induced apoptosis, enhance invasion through its physical association with matrix metalloproteinase-9 and to promote *in vivo* tumor growth with poor prognosis (14). *LCN2* is also reported to promote various cancers by inducing EMT via signaling (12-21). Furthermore, *LCN2* promotes EMT that facilitates an invasive tumor phenotype and metastasis. Therefore, *LCN2* can be considered as a potential diagnostic/prognostic marker for cancer progression.

Lung cancer is an aggressive disease with very high mortality rates (22). Refined studies on the mechanisms of tumorigenesis and chemoresistance of lung cancer are needed to improve the survival rate. Adenocarcinoma of lung exhibits a very low survival rate especially in *LCN2*-A549 lung cancer (13,23). Therefore, selective inhibitors with no cytotoxic effects on normal cells need to be developed for the treatment of lung cancer. Phyto-drug-based approaches provide avenues to ameliorate therapeutic strategies for effective cancer treatment (24,25). BRM270 is a promising anticancer medicinal plant extract that is widely distributed in Northeast Asia, mainly in China, Korea and Japan (25). Apart from that TICSCs in general, relative to normal cells, demonstrate elevated glucose metabolism but the mechanism for this is unknown. The clinical utility of these biomarkers to detect tumor localization and targeting using image-guided therapy has been limited to the use of 2-[F-18]-fluoro-2-deoxy-D-glucose (FDG or 2DG) and positron emission tomography (PET) to identify cancer tissues (26). The study hypothesis considers the extent to which elevated *LCN2* mediated tumorigenesis and metastasis increase their uptake and metabolism of glucose is predictive of cancer cell susceptibility to 2DG-induced radio-/chemosensitization and oxidative stress in adenocarcinoma of lung. The goal of this study is to provide a novel mechanism-based biochemical rationale for the use of glucose metabolic differences and functional imaging to develop biologically guided combined modality therapies to treat oncogene (such as *LCN2)*-induced carcinogenesis based on tumor specific sensitivity to metabolic oxidative stress.

In the present study, we explored the potential role of *LCN2* in inducing EMT and its cross-talk with the NF-κB signaling pathway. Secondly, the role of *LCN2* in EMT mediated tumorigenesis and adenocarcinoma of the lung in xenograft models was investigated by 2DG optical probe as image-guided therapeutics strategy. In addition, we also sought to establish the novel paradigm of EMT *in vitro* systems and implemented *in vivo* models. Further, tumorigenic ability of $CD133^+$-*LCN2*-A549 TICSCs was also compared with $CD133^+$-A549-TICSCs. The present study potentially targeted on the establishment of a novel therapeutic strategy linking 2DG to *LCN2*-induced EMT and growth promotion of lung cancer cells through cooperation with the NF-κB signaling with zero cytotoxicity to normal tissue against adenocarcinoma of lung through the use of BRM270 as a novel anticancer naturaceutics with 2DG optical probe.

## Materials and methods

*Animal model of EMT induced metastasis*. Nude 6-week-old male BALB/cSIc nu/nu mice were purchased from Japan SLC, Inc. They were housed under uniform environmental and nutritional conditions. Mice were sacrificed at 10-, 11-, and 12-week-age according to the standard protocols of Jeju National University. The research proposal and the relevant experimental procedures were approved by the institutional review board of the Department of Animal Biotechnology, Jeju National University, Jeju Special Self-Governing Province, Korea. All animal studies were conducted to induce tumors. Tumorigenesis induction was performed in 34 nude mice. To study the tumorigenesis and metastasis, the mice were grouped into six groups. Six mice each were used as positive control of EMT (non-*LCN2* transfected A549 TICSCs induced tumor group), the test group of EMT and metastasis (*LCN2*-A549 TICSCs induced mouse group). Also, the 6 mice each were incorporated as a treatment group of EMT (*LCN2*-A549 TICSCs BRM270-treated group) and positive control (Dox-treated group). Four mice were used in a negative control group in which hBMCs were injected. To analyze the tumorigenic efficiency of $CD133^+$ A549 TICSCs and *LCN2*-A549 TICSCs, we injected $5x10^6$ cells/ml concentrations of cells into lower right flanks of nude mouse by micro-needle syringe (29 gauge x 1/2" 12.7 mm needle, Ultra-Thin Plus™ Korea).

*Optical probe guided molecular imaging of tumor metastasis*. For pre- and intraoperative tumor localization in real-time resection, we conducted *in vivo* tumor localization assay using IRDye® 800CW 2-DG (2-deoxy-D-glucose) optical probe which was purchased from LI-COR, Biosciences, USA. To evaluate and establish metastatic potential of A549

vs *LCN2*-A549 TICSCs, characterized cells were inoculated subcutaneously to nude mice. After 7 days experimental metastasis was observed followed by observation of distinct 'spontaneous metastasis', where the tumor cells were first allowed to form a primary tumor at the site of injection and then to escape into lymphatic or blood circulation. Probe was dissolved in phosphate buffer saline (1X PBS) and was injected into the tail vein of the tumor-bearing nude mice then mice were observed after they were anesthetized with Zoletil 50 (Virbac, Carros, France) 1 ml/kg intraperitoneally and all surgical procedures were performed under general anesthesia at different time intervals. Metastasis was detected using optical molecular imaging, in particular near-infrared fluorescence (NIRF) range.

*Propagation of cell lines and reagents*. The human lung adenocarcinoma A549 cell line was purchased from Korean Cell Bank, South Korea (KCBL no. 10,185). Cells were propagated in Dulbecco minimum Eagle's medium (DMEM) with 10% fetal bovine serum (FBS) (Hyclone, UT, USA), 1% antibiotic-antimycotic (Gibco, CA, USA) at 37˚C and 5% $CO_2$ under humidified atmosphere. The cells were sub-cultured after attaining confluency level of 80%. For the current experimental study, the cells in passage 3 were used. The hBMCs procured from a 59-year-old Caucasian male were purchased from Korean Cell Line Bank, Seoul, Korea (KCLB no. 10,246) and then were separated by Ficoll-paque density gradient centrifugation (GE Healthcare). The potential hBMCs were further cultured in RPMI-1640 supplied with 20% FBS, 1% antibiotic-antimycotic and 10 nM epithelial growth factor (E9644-Sigma, USA). To test the properties of A549 cells as TICSCs, they were characterized with human anti-CD133 micro magnetic beads (25). Later, after characterization, cells from the pure colonies were injected subcutaneously on the right lower flank of the nude mouse. Seven days post-injection, palpable tumors were observable.

*Cloning and gene transfer of LCN2 into lung adenocarcinoma A549 cell line*. Primers for the cloning of *LCN2* coding sequence were designed on the basis of the homologous regions of humans (Gene Bank accession no. NC_000009). Primers were designed using primer 3.0 tool for 5'-RACE (rapid amplification of cDNA ends) and 3'RACE to obtain the C-terminal coding region of the *LCN2* gene (F-ATGTCACCTCCGTCCTGTTT, R-GTCAGCTCCTTGGTTCTCC). The polymerase chain reaction (PCR) was performed using cDNA from human A549 cells using Prime Taq Premix (2X), (GenetBio, Korea) in a total volume of 20 $\mu$l mixture. The amplified DNA fragments were subsequently cloned into pUC57. Purified PCR products of *LCN2* was sequenced and compared by Cosmo Genetech, Korea.

For the cloning of LCN2, the plasmid vector PiggyBac was procured (Clontech, USA). For the propagation of plasmid and as a maintenance host, *E. coli* Oneshot® Top10 (Invitrogen, USA) competent cells were used. *Hin*dIII restriction enzyme was used to linearize the vector and later, the respective target gene of human lung carcinoma from A549 cells was picked by PCR. Sub-cloning was performed with cloning primers having restriction enzyme sites for *Eco*RI and *Hin*dIII incorporated in forward and reverse primers, respectively. PCR products were separated on 1.2% agarose gel and were extracted by Expin Gel (GeneAll Biotech, South Korea) extraction kit by following the user guidelines.

*Cell proliferation (EZ-CyTox) assay*. Suspended cells (100 $\mu$l) at density of 5,000 cells/well were seeded in 96-well plate (Nunc™, Wiesbaden, Germany). After 24 h of recovery the cells were incubated in humid atmosphere at 37˚C and 5% $CO_2$ and treated with BRM270. The BRM270 was procured from the Biological Response Modifier International Heath Town Corp., Korea. The cells were treated with varying concentrations of BRM270 such as 15.6-125 $\mu$g/ml and doxorubicin (Dox) 10 $\mu$M/ml in cell cytotoxicity assay while 125 $\mu$g/ml BRM270 in rest of the experiments were incubated for 24 h. The enhanced cell viability assay was conducted with EZ-CyTox kit (Daeil Lab Service Co. Korea) to measure the viable cells. EZ-CyTox solution (10 $\mu$l) was added to each well and then cells were incubated for 4 h at 37˚C and 5% $CO_2$. The light absorbance was determined at 450 nm by the Model 680 microplate-reader (Bio-Rad).

*DNA fragmentation assay*. $CD133^+$ A549 and *LCN2* transfected A549 TICSCs ($1x10^6$ cells) were seeded in 6-well microtitre plate (NuncNunclon™ Delta, USA). Then the cells were treated with the 125 $\mu$g/ml concentrations of BRM270 for 24 h for analysis of genomic DNA fragmentation, shrinkage as in our previous study (25). Later, the cells were washed with 1X phosphate-buffered saline (Gibco, Life Technologies™, USA) and were fixed with 4% paraformaldehyde for 10 min followed by incubation with 50 $\mu$M Hoechst 33258 staining solution for 5 min. After three washes with cold PBS, the cells were viewed under a fluorescence microscope (IX-70-Olympus, Japan). Then, genomic DNA was extracted by AccuPrep® Genomic DNA Extraction kit (Bioneer). DNA (5 $\mu$g) was separated on a 1.2% agarose gel. DNA in the gel was stained with ethidium bromide (EtBr) and was visualized under UV light.

*Flow cytometry and cell cycle analysis*. The analysis of cell cycle was detected by PI staining and analysis was performed by flow cytometry using a fluorescence-activated cell sorting (FACS) caliber (Becton-Dickinson). Subsequent to the treatment with 100 $\mu$g/ml and 10 $\mu$M/ml concentrations of BRM270 and Dox for 24 h, $CD133^+$ expressing A549 and *LCN2*-A549 TICSCs were harvested at concentration of $1x10^6$ cells/ml. The cells were fixed in 70% ethanol and incubated at 4˚C overnight. The fixed cells were washed twice with cold PBS and then incubated for 30 min with ribonuclease A (#R-5125, Sigma, 8 $\mu$g/ml) and PI (10 $\mu$g/ml). Then the cell samples were transferred to meshed blue capped tubes (BD Falcon™ Tubes #352235). Later, the fluorescent signals were detected through the FL2 channel and the proportion of DNA that was present in the various phases was analyzed using ModfitLT Version 3.0 (Verity Software House, ME, USA).

*Analysis of EMT induced metastasis by immunocyto/histochemistry (ICC)*. Cultured $CD133^+$*LCN2*-A549 and A549 TICSCs were washed and fixed in 4% phosphate-buffered paraformaldehyde for 25 min at room temperature (RT) then washed three times with cold 1X PBS and permeabilized with

1% Triton X-100 in PBS for 15 min at RT. After washing three times with PBS, the cells were treated with 1% BSA (Sigma, UK) in PBS for 1 h before incubation with primary antibodies in 1% BSA overnight at 4˚C. The cells were then washed with 0.2% Tween-20 (Sigma) in PBS before addition of appropriate FITC-conjugated secondary antibody reagents for 1 h at RT in the dark. Cells were then washed with cold PBS and were counterstained with 4', 6-diamidino-2-phenylindole (DAPI, Invitrogen). After incubation for 5 min, the cells were again washed with cold 1X PBS, and 1 ml mounting media was added and then observed under the fluorescence microscope (Olympus, Milan, Italy) with adaptable filter consistent with Alexa Flour 488, Alexa Flour 546, GFP (green fluorescence protein) and phycoerythrin (PE).

*RNA isolation and quantitative real-time PCR (qPCR).* Cells were seeded at a density of $2x10^6$ cells/T25-mm flask (Nunc, Thermo Scientific, Korea) and were continuously sub-cultured until passage three (P-3) in T75-$mm^3$ flask. At 70% confluency after incubation for 24 h, the culture medium was replaced with RPMI-1640 containing 2% FBS. The cells were detached by trypsin-EDTA 0.5% (Gibco, USA) and total RNA was extracted by easyBlue (Intron Biotech, Korea). The purified RNA was quantified by using Photometer (Bio-Rad, Hercules, USA). Purified RNA (1 $\mu$g) was subjected to first strand c-DNA synthesis using Superscript-III first-strand c-DNA synthesis kit and Oligo(dT) primer (Invitrogen). The c-DNA was subjected to qRT-PCR for the quantification of the relative transcript levels of, h*LCN2*, E-cadherin, Vimentin, Twist-1, TJP-1, SNAI2, p65, and c-Myc using the specific primers which were procured from Cosmo Genetech.

*Quantitative western blotting.* The cells were plated in 60-mm plates and allowed to grow overnight. The cells were then placed in low serum medium (1% FBS) for 16 h, after which the medium was replaced with low serum medium containing either 10% FBS with G418 or only 10% DMEM. To mitigate tumorigenesis in *LCN2*-A549 and A549-injected mice, BRM270 treatment was given to the nude mouse at the rate of 5 mg/ml/day for 2-4 weeks. Total proteins were isolated by ice-cold radioimmunoprecipitation assay (RIPA) buffer supplied phenyl-methane-sulfonyl-fluoride (PMSF) (Sigma-Alrich, USA) and ready to use protein inhibitor cocktails (Fermentas Thermo Scientific, IL, USA). Protein concentrations were calculated by using Pierce® BCA Protein Assay kit (Thermo Scientific) following the manufacturer's instructions. Forty micrograms of proteins were then loaded per well. Proteins were separated on 12% polyacrylamide gel and transferred to polyvinyl-denedi-fluoride membranes (PVDF; Sigma-Alrich Corp., USA) in the Bio-Rad western blot system (Bio-Rad, Berkeley, CA, USA). The membrane was incubated with the primary antibodies (NF-κB, *Lipocalin-2*, E-cadherin, Vimentin, SNAI2, Twist-1, MMP-9, TJP-1 and SMC2 rabbit polyclonal) with control β-actin for overnight and then incubated for one hour with secondary antibodies. All antibodies were procured from Santa Cruz Biotechnology, Inc., CA, USA. The proteins of interest were detected by an enhanced chemiluminescence detection kit following the manufacturer's instructions using LAS400 machine (GE Healthcare, NJ, USA).

*Statistical analyses.* The relative quantitative expression of the genes by real-time qPCR and western blotting was analyzed by the analysis of variance (ANOVA). Kaplan-Meier curves of overall survival of mice were analysed log-rank (Mantel-Cox), and Gehan-Breslow-Wilcoxon test using GraphPad Prism 6 software (CA, USA). In the *in vivo* xenograft tumorigenesis, after day 7 of injection tumor was visible. The tumor was measured with Vernier's calipers and the volume of the tumor ($mm^3$) was calculated by the following formula:

$$\text{Volume} = (\text{width})^2 \left(\frac{\text{length}}{2}\right)$$

Further, the size and the extent of metastasis of tumor under *in vivo* conditions was detected using 2DG-infrared-guided imaging by LI-COR pearl small animal image analyzer (LI-COR Biosciences, USA). All the mice were sacrificed for the collection of tumor samples. The significant differences between the mean expressions of different genes at $P<0.05$ and $P<0.001$ were analyzed by Tukey's b-test. The values are expressed as mean ± SEM.

## Results

*Overexpression of LCN2 is directly associated with CD133 expression and induces an EMT-like morphology leading to metastasis in A549-TICSCs.* To systematically identify candidate differentially expressed genes (DEGs) in EMT, the EMT-inducing *LCN2* expressing $CD133^+$-A549-TICSCs were established using the Nucleofector™-Amaxa Lonza System. Compared to control cells transfected with $p^{maxGFP}$, overexpression of *LCN2* changed the cell morphology in DMEM/F12 supplemented with 10% FBS (Fig. 1A and B). The *LCN2* overexpression leads to the secretion of multiple soluble factors that markedly transform cancer cells into EMT-induced TICSCs. It causes a phenotypic switch leading to an elongated mesenchymal morphology (Fig. 1B). Further, *LCN2* was transfected into $CD133^+$-A549-TICSCs and both *LCN2*-A549 and untransfected A549 cells were analyzed. Immunocytochemistry (ICC) confirmed the expression of *LCN2* in the transfected $CD133^+$-A549-TICSCs. Compared to non-transfected cells, significant changes were observed in the epithelial cell morphology to mesenchymal morphology (Fig. 1B). As expected, the results revealed higher expression of *LCN2* in *LCN2*-A549-TICSCs than in non-transfected A549 cells (Fig. 1C). qPCR and blot expression also demonstrated significantly ($P<0.05$) increased mRNA and protein levels for *LCN2*-A549-TICSCs compared to normal A549-TICSCs and BRM270 treated *LCN2*-A549-TICSCs (Fig. 1D and E). $CD133^+$-A549-TICSCs efficiently induced tumors in male nude mice that were detected using 2DG infrared optical probe by LI-COR image analyzer (Fig. 1F). Moreover, $CD133^+$-A549 and *LCN2* A549-TICSCs were tumorigenic in nature, but *LCN2*-A549 induced long-term growth of solid primary tumors, metastasis initiation and poor prognosis in response to Dox treatment.

*The novel NF-κB inhibitor BRM270 mitigates LCN2 induced metastatic proliferation by downregulation of $CD133^+$-Cyclin D1 mediated premature apoptosis and DNA catastrophe.* Mitotic catastrophe and programmed cell death

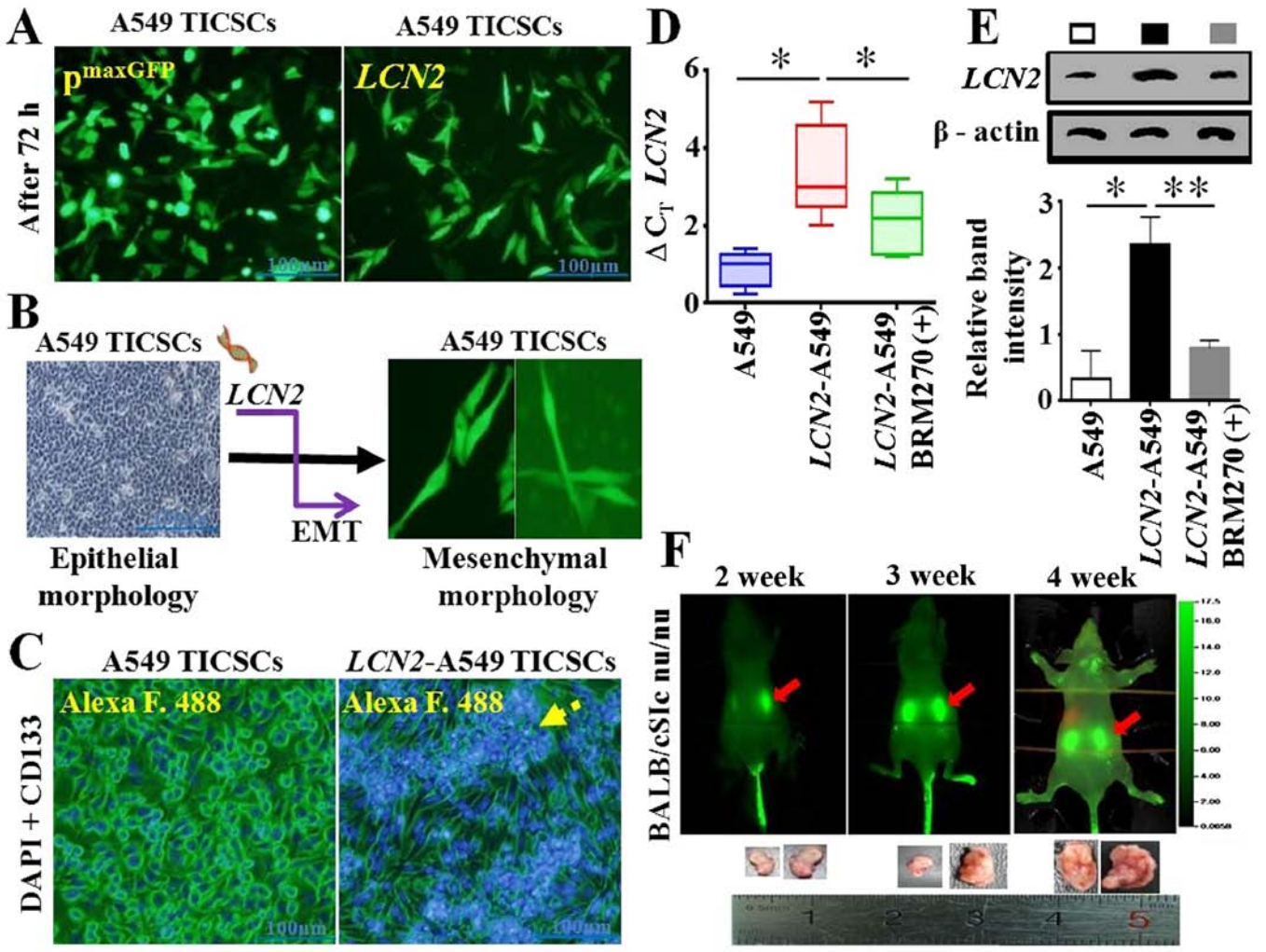


Figure 1. *LCN2* modulates epigenetic switching in CD133$^{+}$-A549-TICSC-induced tumorigenesis. (A) The transfection efficiencies of *LCN2* and p$^{maxGFP}$ in A549 cells were detected by a fluorescence microscope (x100). (B) Genetic transformation of A549-TICS to epithelial-to-mesenchymal under the influence of *LCN2*. (C) ICC analysis of CSC marker CD133$^{+}$ in the transfected A549-TICSCs to show enhanced metastatic cells (yellow arrow). (D) Whisker and Box plot representing mRNA levels of *LCN2* in CD133$^{+}$-TICSCs. (E) Quantitatively blot expression and relative band intensity of *LCN2*. (F) Detection of tumors in BALB/cSIc-(nu/nu) nude mice using IRDye-800CW-2DG optical probe (LI-COR, pearl image system).

in cancer are the most important mechanisms for eradication of TICSCs. It was observed that overexpression of *LCN2* induced stemness in *LCN2*-A549-TICSCs. Specifically, FACS analysis showed that CD133 expression was considerably increased in *LCN2*-A549-TICSCs (4.23%) compared to non-*LCN2* expressing A549-TICSCs (0.79%) (Fig. 2A). Similarly, qPCR showed that transcript levels of CD133 were significantly higher in *LCN2*-A549 TICSCs than A549 and BRM270 treated (Fig. 2B). Furthermore, a reduced ability to form tumor spheres was observed in A549-TICSCs compared to *LCN2*-A549-TICSCs, indicating that *LCN2* drives tumor formation in A549-TICSCs (Fig. 2C). Efficacy of BRM270 exerts anticancer activity. To elucidate the cell shrinkage, morphological DNA fragmentation and programmed cell death by BRM270, we conducted a dose-dependent BRM270 treatment compared to Dox. The CD133$^{+}$-A549 and *LCN2*-A549 TICSCs treated with BRM270 for 24 and 48 h, were stained with Hoechst 33258 and ICC to analyze the extent of genomic DNA fragmentation and cleavage of chromosomal DNA at inter-nucleosomal sites, interruption of microtubule cytoskeletal formation in Dox-resistant TICSCs, as well as the formed chromosomal condensation (pyknosis) and multinucleated fragmentation (karyorrhexis) (Fig. 2D and E, red-yellow-arrows). A dose-dependent viability assay showed that BRM270 caused significantly more cytotoxicity, which was mediated by DNA cleavage and cell death (Figs. 2E and 3A and B). An EZ-WST-Cytox cell proliferation assay (ECPA) in a time-dependent manner showed decreased viability of *LCN2*-A549-TICSCs and confirmed the potential of BRM270 as an anticancer inhibitor. At a concentration of 100 $\mu$g/ml for 12, 24, 48 and 72 h cell viability relative to control A549-TICSCs was calculated as 32.10, 10.46, 3.12 and -11%, respectively. Similarly, 10 $\mu$M exposure of Dox for the same duration resulted in 34.10, 26.22, 12.21 and 9.21% viable *LCN2*-A549-TICSCs, respectively. The cell viability assay of hBMCs, confirmed lesser cytotoxic effect of BRM270 with higher percentage of viable cells i.e. 98.21, 96.25, 97.01 and 96.12%, respectively, as compared to the control. Dox treatment of hBMCs under similar conditions demonstrated 93.12, 92.32, 95.01 and 94.13% cell viability, respectively. It further

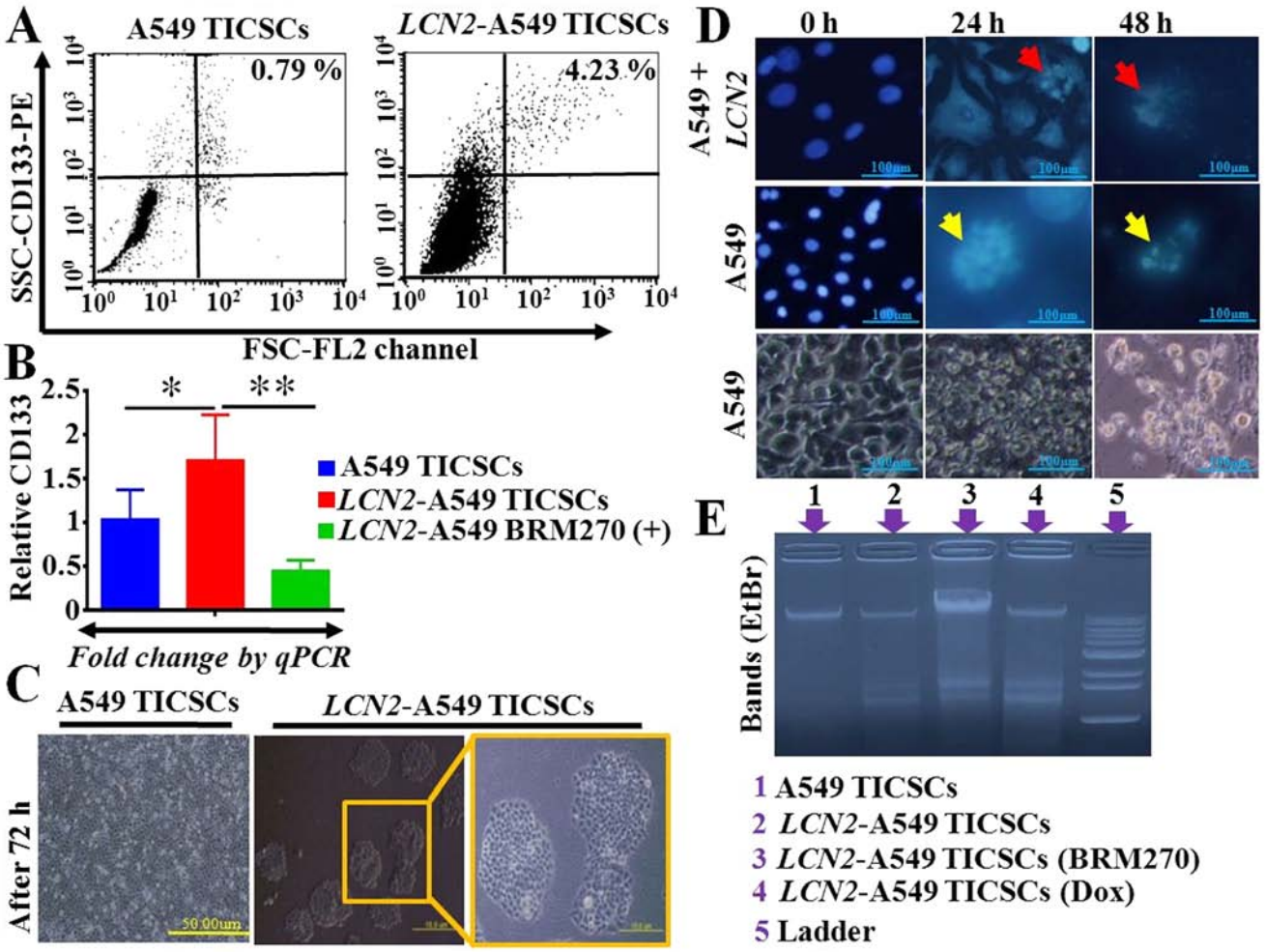


Figure 2. The NF-κB novel inhibitor BRM270 abrogates metastatic TICSCs via DNA fragmentation and cell shrinkage. (A) Characterization of CD133⁺-A549-TICSCs stained with CD133-PE by flow cytometry. (B) qPCR analysis of CD133⁺ in both TICSCs with or without BRM270. (C) Tumor sphere forming and colonogenicity efficiency of CD133⁺-*LCN2* transfected A549-TICSCs. (D) DNA fragmentation after condensation and shrinkage of cells with Hoechst 33342 staining (blue). The untreated TICSCs are flat with oval-shaped nuclei uniformly blue; the nuclei of early apoptotic cells lobular or fragmented blue bodies as Karyorrhexis (red-yellow-arrows). (E) Genomic DNA fragmentation of A549 and *LCN2*-A549 TICSCs exposed to BRM270 with different concentration for 24-h exposure. DNA laddering formation was viewed on ethidium bromide-stained gels (1.2%).

confirmed significantly (P<0.05) higher toxicity by Dox than BRM270. In addition, elevated *LCN2* mediated induced stemness of A549 TICSCs was also significantly abrogated by BRM270 via activation of condensation and catastrophe by suppression of CD133 and recruitment of Condensin-I (SMC2) complex (Fig. 3C and D). To address the potential role of BRM270 in regulation of cell cycle progression, cell cycle analysis was performed by FACS. The cell cycle progression is highly regulated at several checkpoints; BRM270 selectively inhibits cell proliferation via Cyclin D1 (CCND1) targeted cell cycle arrest and induces G2/M transition (Fig. 4A and B). It significantly (P<0.05) showed decreased Cyclin D1 via recruitment of proapopotic Casp-3 in transcriptomic analysis (Fig. 4C and D).

*BRM270 abrogates LCN2-induced EMT and downregulates Twist-1 expression, thereby affecting NF-κB trafficking in lung adenocarcinoma*. EMT plays a pivotal role in promoting metastasis in epithelium-derived carcinomas such as adenocarcinoma of the lung via multistep developmental programs. To study the *in vitro* and *in vivo* induction of EMT in adenocarcinoma of the lung, CD133⁺ expressing A549-TICSCs for EMT markers were examined by ICC. Overexpression of *LCN2* was strongly associated with epithelial-derived-mesenchymal solid tumors. Significantly higher *LCN2* expression in transfected A549-TICSCs induced mesenchymal phenotypic induction (Figs. 1B-F and 5A). E-cadherin and tight junction protein-1 (TJP-1) also have shown lesser expression in transfected cells (Fig. 5A). Consequently, the loss of both epithelial maintaining proteins led to the phenotypic reversion of *LCN2* transfected A549-TICSCs to a mesenchymal morphology (Figs. 1B and 5A-C). However, overexpression of *LCN2* stimulated the expression of the oncoprotein Twist-1 and Vimentin in *LCN2*-A549-TICSCs (Fig. 5A). A critical role for SNAI2 and Twist-1 in mediating the oncogenic functions of *LCN2*, as well as the molecular changes related to EMT markers are highlighted in the present study. Targeted induction of SNAI2 and Twist-1 efficiently reduced the expression of epithelial marker proteins, which could play a role in promoting *LCN2*-induced EMT in A549-TICSCs (Fig. 5A). The transcript levels of EMT-related genes SNAI2 (F-CCTGGTTGCTTCAAGGACAC, R-AGCAGCCAGATTCCTCATGT), Twist-1 (F-TCC

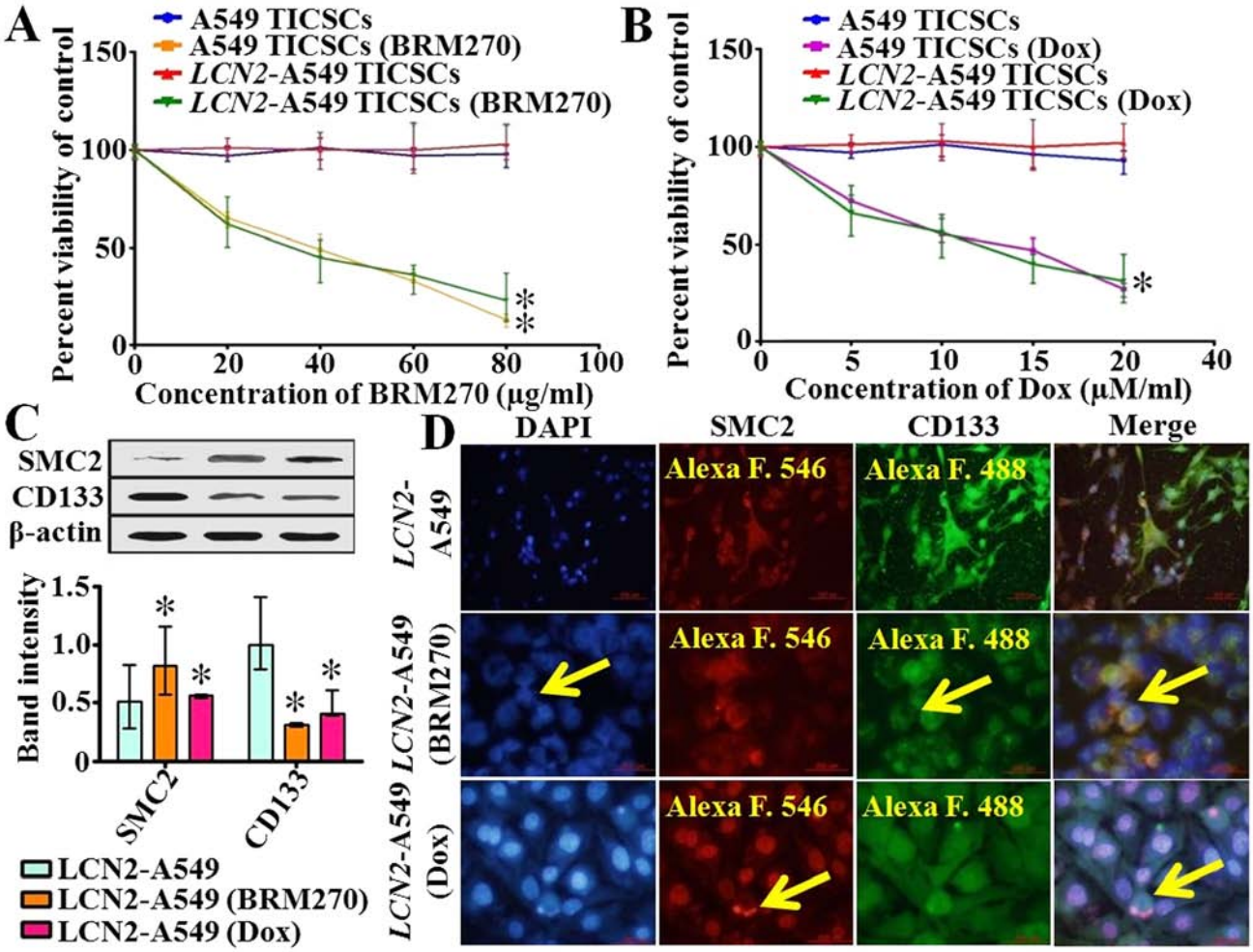


Figure 3. The novel NF-κB inhibitor BRM270 inhibits cell proliferation via targeting of Condensin (SMC2)-I complex in CD133$^+$ overexpressing *LCN2*-A549 TICSCs in a dose-dependent manner. (A and B) The percent viability of TICSCs by EZ-CyTox cell proliferation test. (C) Total lysates were immunoblotted for SMC2-mediated cell shrinkage and catastrophe in TICSCs. (D) Protein-protein interaction and localization by ICC that showed DNA fragmentation and PCD counter stained with DAPI (blue DNA).

TCACACCTCTGCATTCT, R-ATGGTTTTGCAGGCCA GTTT) (P<0.05), involved in maintaining the mesenchymal phenotype were significantly (P<0.001) higher in *LCN2*-A549-TICSCs than in A549-TICSCs (Fig. 5B). On the contrary, a significant reduction in the transcript levels of E-cadherin (F-GCTGGAGATTAATCCGGACA, R-ACCTGAGGCTT TGGATTCCT) and TJP-1 was detected in *LCN2*-A549-TICSCs compared to A549-TICSCs (Fig. 5A and B).

It was observed that after 24 h, BRM270 (100 $\mu$g/ml) strongly (P<0.001) downregulated the expression of mesenchymal biomarkers as compared to Dox (Fig. 5B). The essential diatomous phenomenon of EMT induced by *LCN2* was investigated. Further, it has been observed that *LCN2* induces a biochemical hallmark of EMT, which is loss of expression of epithelial markers with a concurrent increase in the expression of mesenchymal markers (Fig. 5C). Western blot analysis demonstrated that BRM270 significantly down-regulated (P<0.001) the tumorigenic EMT induced protein Vimentin and increased E-cadherin in both TICSCs compared to untreated cells (Fig. 5D). Moreover, blot analysis of proteins also demonstrated that BRM270 significantly suppressed (P<0.05) the expression of oncogenic proteins as compared to untreated cells (Fig. 5C and D). Collectively, our findings suggest that *LCN2* induces EMT in A549-TICSCs and exhibits *in vitro* as well as *in vivo* capacity to induce metastasis via the appropriate signaling cascade.

*BRM270 abrogates LCN2 mediated invasion and metastasis in a molecular imaging in vivo model of adenocarcinoma of the lung*. The expression of *LCN2* is upregulated in cancer and it enhances formation, progression, and metastasis of adenocarcinoma of the lung. To evaluate whether *LCN2* augments tumor growth and metastasis *in vitro* and *in vivo*, the cell culture of CD133$^+$ both TICSCs were optimized to generate cells to induce high-grade solid tumors in nude mice. Both cell lines were injected subcutaneously, ortho-topically into the lower right flank of male nude mice (Fig. 6A). Tumor formation and metastasis were confirmed *in vivo* using a small animal image analyzer system. CD133$^+$-*LCN2*-A549-TICSCs efficiently induced the tumors and metastasized to other organs, while A549-TICSCs induced only localized tumors and did not metastasize (Fig. 6B). Infra-red (IR) dye-800CW-2-deoxy-D-glucose (2DG) wavelength-based images were taken at different time intervals (2-, 3- and 4-week) to monitor

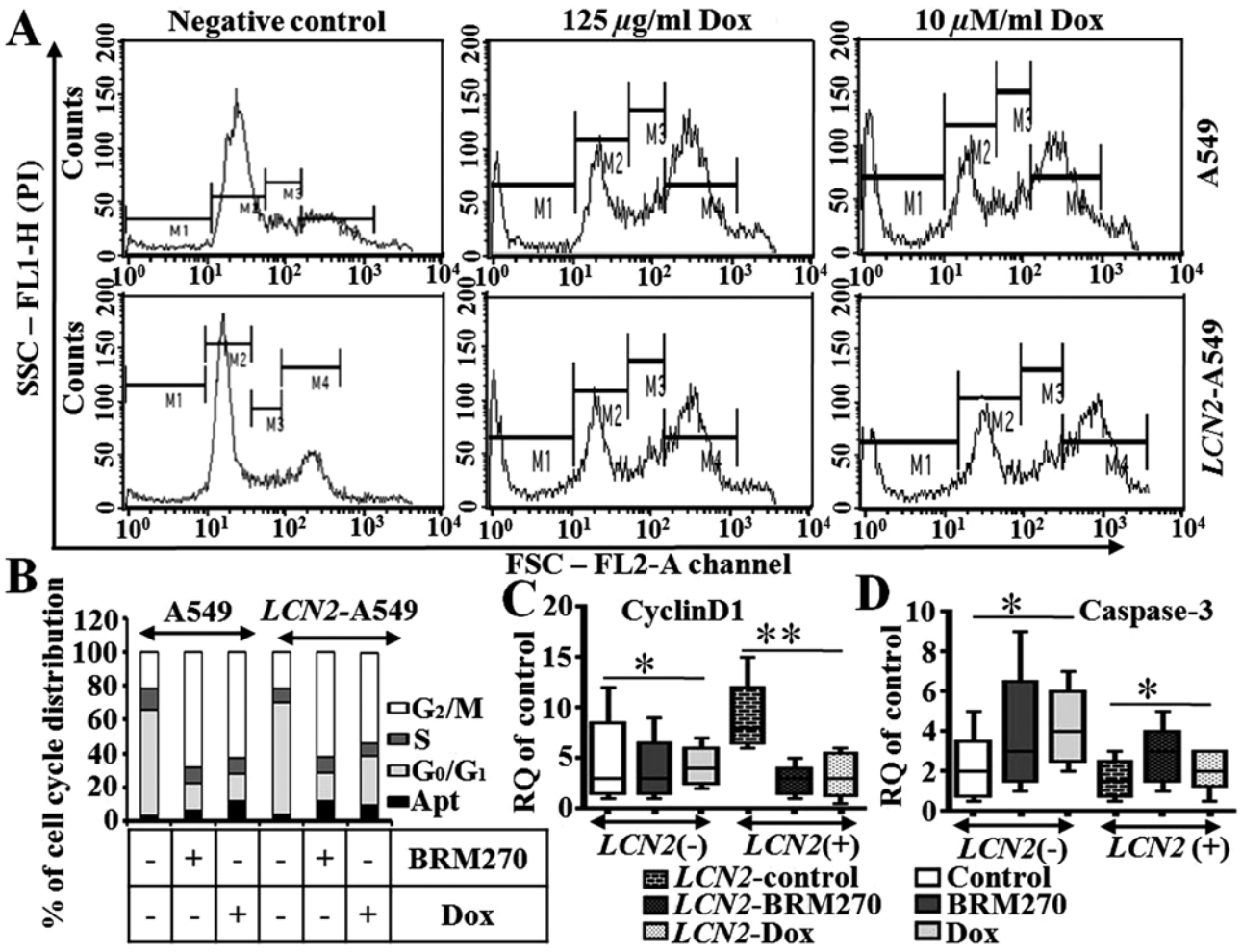


Figure 4. Influence of BRM270 on cell cycle progression and apoptosis in TICSCs. (A) Cell cycle analysis of $CD133^{+}$-A549 and *LCN2*-A549-TICSCs after being cultured with BRM270 for 24 h showing an increase in G2/M phase cells (%). (B) Percent of cell cycle distribution in different checkpoints: flow cytometry analysis showing G0-G1 arrest and transition to G2M checkpoints. (C and D) mRNA fold change of Cyclin D1 and procaspase-3 with or without BRM270 compared to Dox.

tumor progression (Fig. 6B). 2DG was used as a tracer for identification of tumors and their metastases because the rate of glycolysis is elevated in highly proliferative tumors and metastasized organs. The tumors were detectable at day 7 after the implantation of both TICSCs in nude mice. The tumor signal intensity was significantly (P>0.05) higher in *LCN2*-A549 tumors than A549 tumors at third and fourth weeks, respectively, indicating that *LCN2*-A549 tumors were larger (Fig. 6B). To ascertain that *LCN2* mediates tumor cell proliferation and metastasis, tumor growth patterns were analyzed in both implanted groups. The results of *in vivo* experiment confirmed that BRM270 significantly (P<0.05) inhibited tumor progression in a dose- and time-dependent manner. It also had a positive impact on disease prognosis compared to Dox treated mice (Fig. 6B). Further, $CD133^{+}$-*LCN2*-A549-TICSC tumor-bearing mice displayed a significantly (P<0.0003) lower relapse-free survival rate (11.4286%) than A549-TICSCs tumor-bearing mice (30.2098%) (Fig. 6C). BRM270 significantly (P<0.0005) increased the prognostic value and enhanced the survival rate of *LCN2*-A549-TICSCs in tumor-bearing mice from ~40 to 65.625% compared to Dox treated mice (57.2727%) in 2DG guided *in vivo* model (Fig. 6C).

To support our findings, we compared the weights of tumors in both groups. It was observed that *LCN2*-A549-TICSCs were more invasive and metastatic in nature because the tumor weight increased significantly (P<0.05) between the second and fourth week (P<0.001). However, BRM270 significantly reduced the volume of tumor over time as compared to untreated mice (Fig. 6D and 7A). Significantly (P<0.001) enhanced reduction in tumor weight was observed with BRM270 at a dose rate of 10 mg/kg/day twice a week (Fig. 7Ae). The mean tumor volume of A549 and *LCN2*-A549-TICSC tumors was measured (Fig. 7B). Post-inoculation on day 7, a marked difference in tumor volume and onset of metastasis was observed. Surprisingly, at day 9 the palpable tumors of A549-TICSCs grew at a significantly slower (P<0.05) rate than *LCN2*-A549-TICSC tumors (Fig. 7B). A significantly lower average volume of metastatic tumors was observed in both BRM270 treated A549 and *LCN2*-A549 tumor-bearing mice (Fig. 7B). Histological analysis of metastatic tumor samples demonstrated significantly higher proliferation rate of *LCN2*-A549-TICSCs than A549-TICSCs (Fig. 7C). The correlation of the relative body weight with tumor metastasis and amelioration by BRM270 showed a

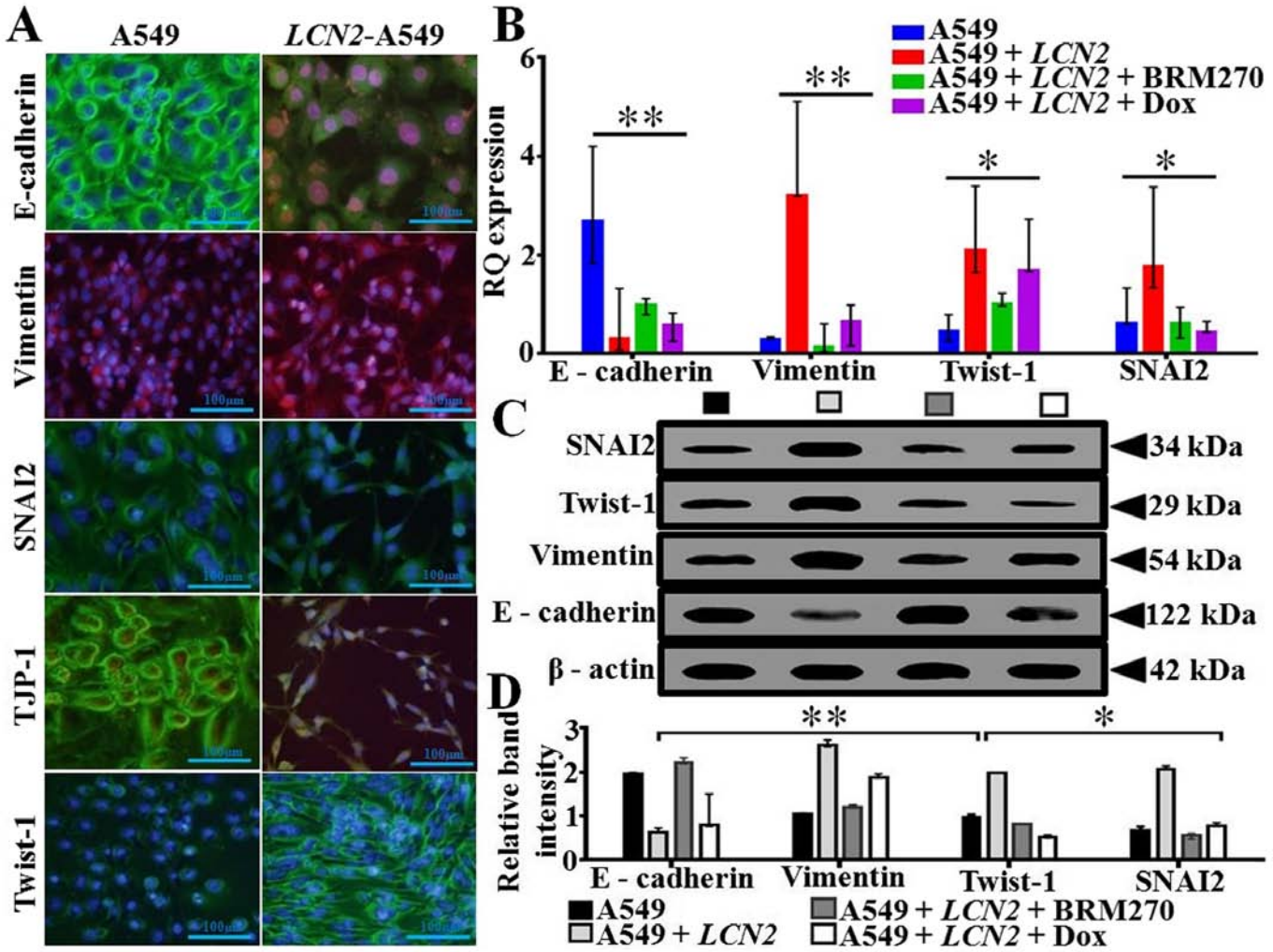


Figure 5. *LCN2* augments SNAI2/Twist-1 mediated EMT and phenotypic reversion in lung adenocarcinoma. (A) ICC for EMT inducing proteins with DAPI counterstaining for DNA (blue, x200). (B) Summary of gene expression switches with qPCR showing mean fold change in mRNA abundance. (C) Total lysates were immunoblotted for EMT markers in TICSCs and BRM270 treated with the positive control Dox. (D) The image densitometry analysis by ImageJ.

significant reduction in body weight in high grade metastasized tumor-bearing mice (Fig. 7D). It was also confirmed that while acting as novel anticancer phyto-drug, BRM270 does not significantly affect relative body weight of mice compared to Dox. Taken together results revealed that *LCN2* overexpression correlates with tumor malignancy, metastasis and mediates adenocarcinoma of the lung.

*The LCN2-Twist-1/MMP-9 interaction mediates EMT cross-talk with the NF-κB signaling cascade*. It was targeted that *LCN2* regulates cell-cell adhesion, EMT induced metastasis, followed by cross-talk with the NF-κB signaling pathway (Fig. 8A and B). To define the molecular mechanism of *LCN2*-mediated EMT, a cancer-associated protein-protein interaction network was constructed using STRING bioinformatics approach (Fig. 8A). The results showed that *LCN2* binds to MMP-9 that is activated by SNAI2 and is involved in Twist-1 activated EMT. Overexpression of *LCN2* directly increased MMP-9 expression, and it was also activated by the mesenchymal EMT markers (Fig. 8A). The results were further confirmed by western blotting and subsequent densitometry quantification of protein expressions. We found that *LCN2* induction negatively regulates both E-cadherin protein interaction and mRNA fold change levels (Fig. 5A-C and 8A). In agreement with the role of NF-κB signaling cascade in mediating MMP-9 interaction, immunoblot and transcriptomic analysis revealed that $\Delta C_T$ levels of NF-κB (F-CTGAACCA GGGCATACCTGT, R-GAGAAGTCCATGTCCGCAAT) and MMP-9 simultaneously with *LCN2* were significantly ($P<0.001$) downregulated with BRM270 treatment compared to Dox (Fig. 8B-D). ICC and qPCR also showed that protein expression and mRNA levels of MMP-9 and NF-κB in both group samples were significantly reduced after 24-h exposure with naturaceutics BRM270 (Fig. 8E and F). It was observed that *LCN2* induced the expression of MMP-9 and Twist-1 and elevated protein interaction in high-grade tumors, indicating that co-expression of NF-κB and Twist-1 enhances the aggressive and metastatic mesenchymal phenotype of A549-TICSCs (Figs. 1B, 5B and 8F). Collectively, these results suggest that *LCN2* induced EMT via NF-κB-MMP-9 interaction in A549-TICSC-induced lung carcinoma. The novel naturaceutic BRM270 anticancer activity elucidated that overexpression of

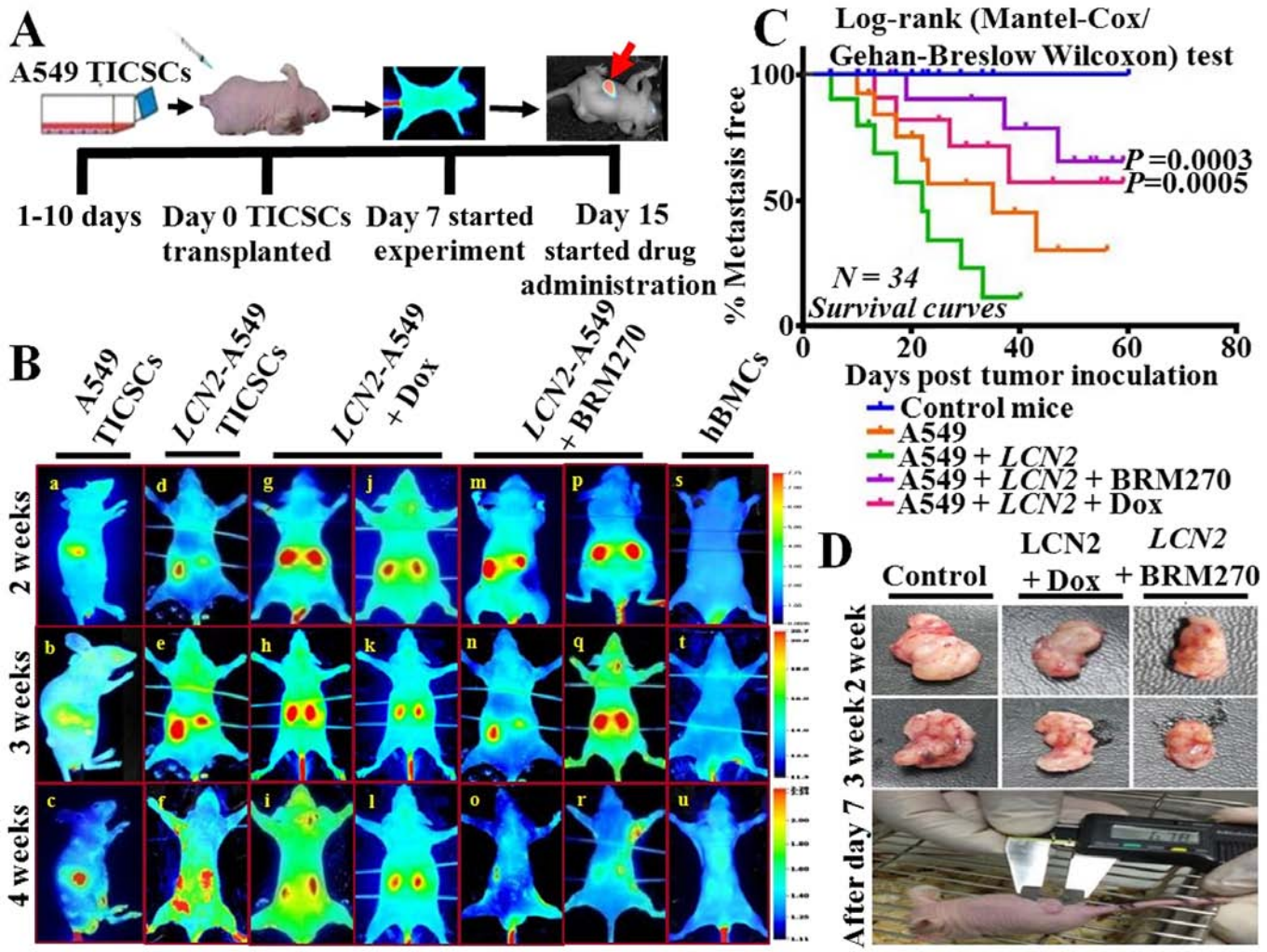


Figure 6. 2DG-guided molecular imaging based *in vivo* model of adenocarcinoma of the lung. (A) Establishment, characterization of metastatic TICSCs and their subcutaneous inoculation into nude mice. (B) Analysis of $CD133^{+}$-TICSC-induced palpable solid tumors and metastasis in male BALB/cSIc-(nu/nu) nude mice, under *in vivo* conditions using LI-COR image analyzer. (C) Progression-free survival curve was calculated with the Kaplan-Meier method and compared by using the log-rank test. ***P<0.0003 and 0.0005 considered as extremely significant of control and treated group. (D) *In vivo* and *ex vivo* measurement of the volume of tumors.

*LCN2* induced adenocarcinoma of the lung and metastasis of high-grade solid tumors can be eradicated using novel nutraceutics.

## Discussion

Stem cell research is a promising arena for the therapeutic advancement in oncology including lung cancer (1-3). EMT, an essential normal physiological process for embryonic development, tissue remodeling and wound healing, has recently been implicated in cancer progression (7-9). Epithelium-derived tumors switch to a mesenchymal phenotype that facilitates migration and invasion potential resulting in increased tumor aggressiveness, recurrence and overall poor prognosis (4,9). We hypothesized that EMT was the likely mechanism by which *LCN2* increased cell migration and invasion as well as tumorigenesis in adenocarcinoma of the lung *in vitro* and in 2DG guided *in vivo* model (Figs. 5A and 6B). Epigenetic induction of EMT in TICSCs is positively correlated with poor prognosis, metastasis, motility and multiple-drug chemotherapeutic resistance (4,20,21). The present study was designed to define the potential of *LCN2* in the switching of EMT in adenocarcinoma of the lung with 2DG infrared optical probe as an *in vivo* molecular tumor tracer. The results showed that, ectopic overexpression of *LCN2* resulted in morphological reversion from the epithelial to the mesenchymal phenotype in A549-TICSCs (Fig. 1A and B). *LCN2* is also known to promote breast cancer progression via downregulation of epithelial markers and the acquisition of mesenchymal markers with TF in infrared optical probe based *in vivo* models (16,27). In the present study, the mRNA levels of *LCN2* were significantly (P<0.05) higher in *LCN2*-A549-TICSCs than in normal A549-TICSCs (Fig. 1D). Overexpression of *LCN2* in A549-TICSCs was confirmed by ICC in both *LCN2* transfected and non-transfected cells (Fig. 1C). Further, enhanced cell proliferation with its overexpression *in vitro* (Figs. 1C and 2C) is supported by earlier literature (15,16). The putative CSC marker CD133 strongly expressed on the cell surface of A549-TICSCs (Fig. 1C) as earlier reported and confirmed the tumor inducing ability (5,6). The higher metastasis and invasive rates in *LCN2*-

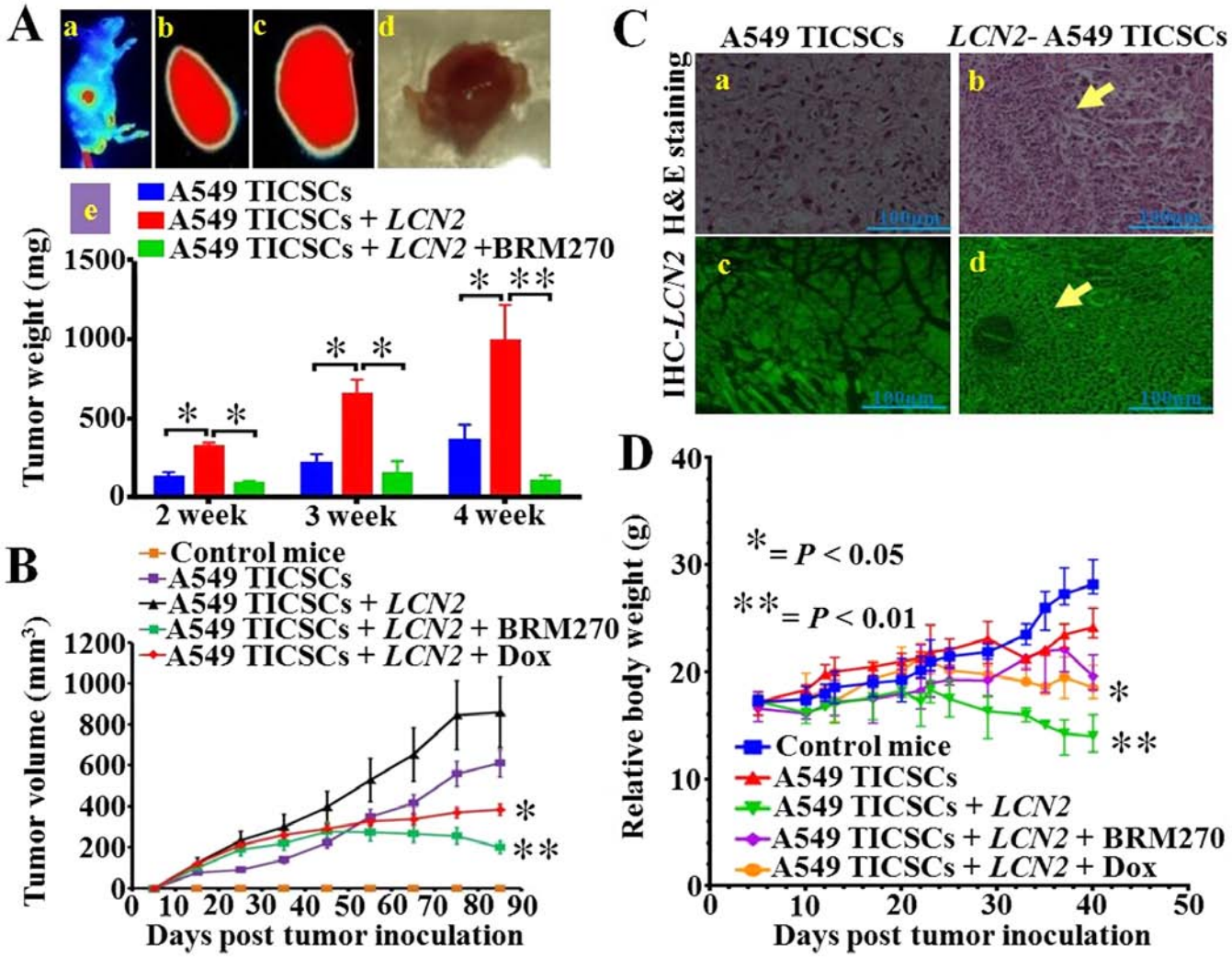


Figure 7. BRM270 reduces tumor extent in a dose- and time-dependent manner. (A) Diagrammatic presentation of relative weight of solid tumors. (B) Representation of tumor volumes over the different time intervals. (C) IHC and H&E staining of *LCN2*-A549 and A549-induced adenocarcinoma of tumor sections-(x20). (D) Relative body growth curves of tumor groups. Data was analyzed using GraphPad prism6.

A549-TICSCs with respect to A549-TICSCs (Fig. 6B) during the present study are supported by the findings of a pancreatic ductal adenocarcinoma xenograft model (20). Further, enhanced stemness, MDR and tumorigenicity under *in vitro* and *in vivo* by *LCN2* was supported by the earlier findings for many cancers especially lung cancer and ductal adenocarcinoma (5,6,16,20,27).

Mitotic catastrophe can induce programmed cell death that often occurs in conjunction with apoptosis. In our previous study, we demonstrated that BRM270 is a potential and selective anticancer phyto-drug that induces programmed cell death and mitotic cell death (MCD) due to unrepaired DNA damage during premature apoptosis (25,28). Further, the efficacy of BRM270 is related to its ability to subdue the mRNA expression of *LCN2* and consequently $CD133^+$ stemness and tumorigenicity of A549 TICSCs (Figs. 2B and C and 6B). The efficiency of BRM270 to significantly abrogate ($P<0.001$) the increased $CD133^+$ expression in A549 and *LCN2*-A549-TICSCs compared to Dox treatment, in a time- and dose-dependent manner, is in line with our previous study (25). DNA catastrophe and MCD are prominent mechanisms in carcinogenesis (25,27), during chemotherapy or cancer progression by premature mitosis and uneven chromatin condensation and BRM270 has significantly facilitated such activities in the present study (Figs. 2D and 3D). In addition, BRM270 is also known to regulate cell cycle arrest and transit from G0-G1 to G2/M checkpoints by Casp-3 via downregulation of Cyclin D1. This is a causal hallmark of premature apoptosis, cells with defective G2/M phase by induction of Casp-3 dependent pro-apoptosis (27,28).

The present study elucidates a pivotal role for *LCN2* in EMT. It also confirmed in line with the earlier studies that overexpression of *LCN2* significantly ($P<0.05$) antagonizes the expression of epithelial markers, upregulates mesenchymal markers (Fig. 5 and 8A) and drives EMT via E-cadherin, SNAI2, Twist-1, NF-κB and MMP-9-dependent and independent mechanisms (7,16,18). As expected, the upregulation of NF-κB induced stemness, tumor sphere formation and metastasis (Figs. 1F, 2C, 6B and 8C). Several earlier studies also indicated that the versatile role of *LCN2* in the early stage of tumor development and its higher expression in ovarian, thyroid, liver, colon, kidney, and pancreas (12,15,29-32).

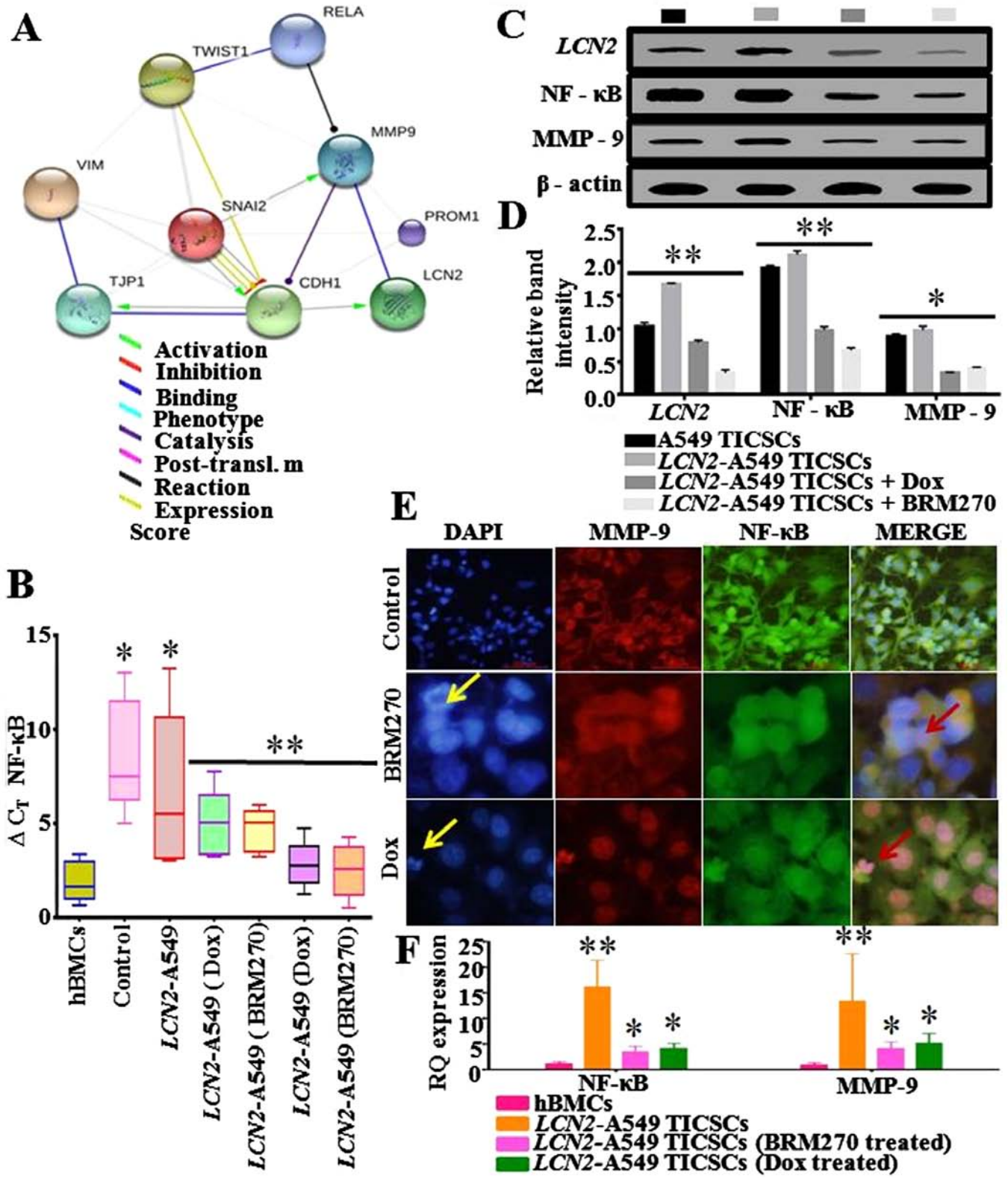


Figure 8. *LCN2* enhances EMT and cross-talk with the NF-κB signaling cascade. (A) Cancer-associated protein-protein interactions network was constructed using the bioinformatics STRING. (B) Whisker and Box plot for NF-κB activity using Data Assist of qPCR analysis. (C) Protein lysates were analyzed by western blotting for NF-κB cross-talk with EMT and their interaction in *LCN2*-induced metastatic tumor. (D) Quantification of band intensities using ImageJ. (E) ICC revealed that the novel inhibitor BRM270 abrogates the protein-protein interaction and cross-talk with NF-κB. (F) qPCR showing the relative significant suppression of both MMP-9 and NF-κB mRNA levels by BRM270. $^{*}$P<0.05, $^{**}$P<0.001 indicate significant differences.

Further it has been observed that elevated transcript levels induced degradation of IκB proteins and resulted in the liberation of NF-κB. It allowed nuclear translocation and binding to cognate DNA motifs that induce transcription of EMT promoting proteins and augment tumor sphere formation in *in vitro* and metastasis *in vivo*. Consequently, transcription of

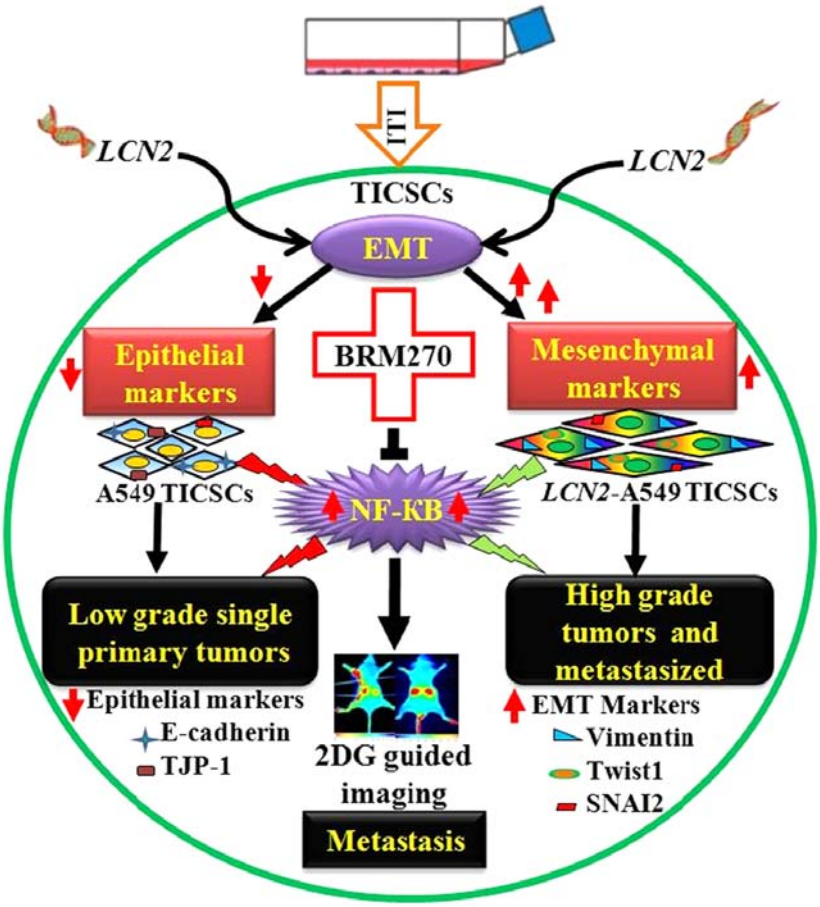


Figure 9. Schematic representation of epigenetic induction of EMT and their cross-talk with NF-κB signaling cascade in lung adenocarcinoma. Representation of BRM270 as a novel inhibitor, amelioration of EMT-mediated cancer progression and metastasis by targeting the Twist-1 and NF-κB using 2DG for pre- and intraoperative tumor localization in real-time resection.

EMT-related genes involved in EMT and cross-talk to NF-κB occurs (Figs. 5 and 8A). The present study demonstrates a functional role for *LCN2* and several known EMT mediators, showing that induction of EMT in adenocarcinoma of the lung proceeds via activation of NF-κB signaling and activation of Twist-1 and SNAI2. Thus it provides new insights into the mechanism of EMT induction in lung carcinoma. Moreover, it shows that BRM270 functions as a novel inhibitor that blocks EMT mediated oncogenesis. Taken together, these results suggest that *LCN2* triggers EMT, which is associated with increased potential for metastasis and invasion.

One of the important and clinically relevant aspects of cancer stem cell tumorigenicity is the degree of cancer spread beyond the primary tumor in various cancers including adenocarcinoma of the lung. The present study suggests that the *LCN2*-transformed A549 TICSCs induced metastatic tumors in nude mice (Fig. 6A and B). Similarly, *LCN2* decreases differentiation and increases breast tumor local invasion, lymph node metastasis and primary tumor growth *in vivo* (29). Our findings also confirmed that *LCN2* regulates a variety of cellular functions in carcinogenesis that could either induce or suppress cancer metastasis and invasiveness (32-36). Further, a significant difference in the baseline tumor volume between the two groups confirmed significantly ($P<0.05$) faster growth rate by *LCN2*-A549-TICSCs than A549 TICSCs (Fig. 7B). This result suggests that *LCN2* has significant oncogenic activity, which is supported by earlier reports (34,36). The findings of Mannelqvist *et al* of 51% survival in tumors with no *LCN2*, 46% in medium *LCN2* expression and 3% in endometrial cancer tumors that strongly express *LCN2* supported our results (35). This suggests that *LCN2* expression leads to poor tumor prognosis and can serve as a biomarker for treatment. *LCN2* causes tumor progression in bladder, colorectal, liver, ovarian and pancreatic carcinoma (15,36), which supports our result of *LCN2* in adenocarcinoma of the lung by 2DG infrared optical probe guided molecular imaging-based *in vivo* model. The novel infrared probe 2DG is a potential molecular navigation therapeutics tracer that detects tumors in real-time intraoperatively in contrasting pseudo-colors, which allows more complete tumor resection (26). Therefore, *in vivo* targeting experiments indicated the 2DG-based complex had great potential for image-guided cancer therapy. This study suggests that *LCN2* have potential as a non-invasive biomarker for metastasized advance cancer progression and 2DG is a novel optical probe to target tumor recurrence and metastasis.

*LCN2* enhances EMT-mediated cancer progression by activation of Twist-1/SNAI2 and cross-talk with the NF-κB signaling cascade, a novel paradigm in most cancers (11,18,32,33). The present study provides evidence for a novel cellular signaling mechanism regarding *LCN2*-induced

EMT and cross-talk with NF-κB in lung carcinoma (Fig. 9). Similarly, Shrivastava *et al* demonstrated cancer-associated expression of MMP-9 and c-FOS with *LCN2* protein network interaction and signaling using the same STRING bioinformatics strategy used in this study (37). In addition, they also demonstrated that the activator protein-1 (AP-1) complex formed by the association of c-Fos and c-Jun was implicated in the maintenance of colon cancer stem cells, which correlates with our findings of the CDH1 and MMP-9 complex with NF-κB (Fig. 8).

This study provides compelling evidence of epigenetic switching of *LCN2*-mediated EMT and cross-talk with NF-κB. Also, it proposes a wide range of strategies by which BRM270 mitigates the progression and metastasis of A549 and *LCN2*-A549-TICSC-induced adenocarcinoma of lung *in vitro* and 2DG infrared optical probe guided *in vivo* model (Fig. 9). Our findings can aid in the identification of molecular mechanisms of carcinogenesis in $CD133^+$-*LCN2* transfected A549-TICSC-induced carcinoma by optical probe guided molecular imaging-based therapeutic strategies in experiments. This information is a novel clinically relevant and can act as the baseline data for the development of new naturaceutics with direct target to resection of tumor and metastasis by image-guided therapeutic strategies. In conclusion, the present study provides a molecular mechanistic and photodynamic-based approach for using BRM270 as a novel cancer therapeutic drug to enhance the effect of Dox-resistant *LCN2*-induced metastasis of solid tumors in nude mice.

## Acknowledgements

The authors thank Next-Generation Bio Green 21 Program organization. This study was supported by Next-Generation Bio Green 21 Program grant number PJ01117401, Rural Development Administration, Republic of Korea.

## References

1. Jordan CT, Guzman Ml and Noble M: Cancer stem cells. N Engl J Med 355: 1253-1261, 2006.
2. Kitamura H, Okudela K, Yazawa T, Sato H and Shimoyamada H: Cancer stem cell: Implications in cancer biology and therapy with special reference to lung cancer. Lung Cancer 66: 275-281, 2009.
3. Wang P, Gao Q, Suo Z, Munthe E, Solberg S, Ma L, Wang M, Westerdaal NA, Kvalheim G and Gaudernack G: Identification and characterization of cells with cancer stem cell properties in human primary lung cancer cell lines. PLoS One 8: e57020, 2013.
4. Rich JN and Bao S: Chemotherapy and cancer stem cells. Cell Stem Cell 1: 353-355, 2007.
5. Bertolini G, Roz L, Perego P, Tortoreto M, Fontanella E, Gatti L, Pratesi G, Fabbri A, Andriani F, Tinelli S, *et al*: Highly tumorigenic lung cancer $CD133^+$ cells display stem-like features and are spared by cisplatin treatment. Proc Natl Acad Sci USA 106: 16281-16286, 2009.
6. Akunuru S, James Zhai Q and Zheng Y: Non-small cell lung cancer stem/progenitor cells are enriched in multiple distinct phenotypic subpopulations and exhibit plasticity. Cell Death Dis 3: e352, 2012.
7. Tsai JH and Yang J: Epithelial-mesenchymal plasticity in carcinoma metastasis. Genes Dev 27: 2192-2206, 2013.
8. Li CW, Xia W, Huo L, Lim SO, Wu Y, Hsu JL, Chao CH, Yamaguchi H, Yang NK, Ding Q, *et al*: Epithelial-mesenchymal transition induced by TNF-α requires NF-κB-mediated transcriptional upregulation of Twist1. Cancer Res 72: 1290-1300, 2012.
9. Casas E, Kim J, Bendesky A, Ohno-Machado L, Wolfe CJ and Yang J: Snail2 is an essential mediator of Twist1-induced epithelial mesenchymal transition and metastasis. Cancer Res 71: 245-254, 2011.
10. Nagai T, Arao T, Matsumoto K, Sakai K, Kudo K, Kaneda H, Tamura D, Aomatsu K, Kimura H, Fujita Y, *et al*: Impact of TJP-1 and TWIST expression on post-operative prognosis in hepatocellular carcinoma, Proceedings of the 103rd Annual Meeting of the AACR. Cancer Res72: 3406, 2012.
11. Huber MA, Azoitei N, Baumann B, Grünert S, Sommer A, Pehamberger H, Kraut N, Beug H and Wirth T: NF-kappaB is essential for epithelial-mesenchymal transition and metastasis in a model of breast cancer progression. J Clin Invest 114: 569-581, 2004.
12. Zhai L, Wang T, Kang K, Zhao Y, Shrotriya P and Nilsen-Hamilton M: An RNA aptamer-based microcantilever sensor to detect the inflammatory marker, mouse lipocalin-2. Anal Chem 84: 8763-8770, 2012.
13. Shi H, Gu Y, Yang J, Xu L, Mi W and Yu W: Lipocalin 2 promotes lung metastasis of murine breast cancer cells. J Exp Clin Cancer Res 27: 83, 2008.
14. Lin CW, Tseng SW, Yang SF, Ko CP, Lin CH, Wei LH, Chien MH and Hsieh YS: Role of lipocalin 2 and its complex with matrix metalloproteinase-9 in oral cancer. Oral Dis 18: 734-740, 2012.
15. Candido S, Maestro R, Polesel J, Catania A, Maira F, Signorelli SS, McCubrey JA and Libra M: Roles of neutrophil gelatinase-associated lipocalin (NGAL) in human cancer. Oncotarget 5: 1576-1594, 2014.
16. Yang J, Bielenberg DR, Rodig SJ, Doiron R, Clifton MC, Kung AL, Strong RK, Zurakowski D and Moses MA: Lipocalin 2 promotes breast cancer progression. Proc Natl Acad Sci USA 106: 3913-3918, 2009.
17. Zhao P, Elks CM and Stephens JM: The induction of lipocalin-2 protein expression in vivo and in vitro. J Biol Chem 289: 5960-5969, 2014.
18. Rodvold JJ, Mahadevan NR and Zanetti M: Lipocalin-2 in cancer: when good immunity goes bad. Cancer Lett 316: 132-138, 2012.
19. Nakamura I, Hama S, Itakura S, Takasaki I, Nishi T, Tabuchi Y and Kogure K: Lipocalin-2 as a plasma marker for tumors with hypoxic regions. Nat Sci Rep 4: 1-8, 2014.
20. Leung L, Radulovich N, Zhu CQ, Organ S, Bandarchi B, Pintilie M, To C, Panchal D and Tsao MS: Lipocalin-2 promotes invasion, tumorigenicity and gemcitabine resistance in pancreatic ductal adenocarcinoma. PLoS One 7: e46677, 2012.
21. Krysan K, Cui X, Gardner BK, Reckamp KL, Wang X, Hong L, Walser TC, Rodriguez NL, Pagano PC, Garon EB, *et al*: Elevated neutrophil gelatinase-associated lipocalin contributes to erlotinib resistance in non-small cell lung cancer. Am J Transl Res 5: 481-496, 2013.
22. Torre LA, Bray F, Siegel RL, Ferlay J, Lortet-Tieulent J and Jemal A: Cancer incidence and mortality worldwide: Sources, methods and major patterns in GLOBOCAN 2012. CA Cancer J Clin 65: 87-108, 2015.
23. Saeed AM, Toonkel R, Glassberg MK, Nguyen D, Hu JJ, Zimmers TA, Robbins DJ, Koniaris LG and Lally BE: The influence of Hispanic ethnicity on nonsmall cell lung cancer histology and patient survival: An analysis of the Survival, Epidemiology, and End Results database. Cancer 118: 4495-4501, 2012.
24. Chen SS, Michael A and Butler-Manuel SA: Advances in the treatment of ovarian cancer: A potential role of antiinflammatory phytochemicals. Discov Med 13: 7-17, 2012.
25. Mongre RK, Sodhi SS, Ghosh M, Kim JH, Kim N, Park YH, Kim SJ, Heo YJ, Sharma N and Jeong DK: The novel inhibitor BRM270 downregulates tumorigenesis by suppression of NF-κB signaling cascade in MDR-induced stem-like cancer-initiating cells. Int J Oncol 46: 2573-2585, 2015.
26. Kovar JL, Volcheck W, Sevick-Muraca E, Simpson MA and Olive DM: Characterization and performance of a near-infrared 2-deoxyglucose optical imaging agent for mouse cancer models. Anal Biochem 384: 254-262, 2009.
27. Choi M, Kim W, Cheon MG, Lee CW and Kim JE: Polo-like kinase 1 inhibitor BI2536 causes mitotic catastrophe following activation of the spindle assembly checkpoint in non-small cell lung cancer cells. Cancer Lett 357: 591-601, 2015.
28. Mantena SK, Sharma SD and Katiyar SK: Berberine, a natural product, induces G1-phase cell cycle arrest and caspase-3-dependent apoptosis in human prostate carcinoma cells. Mol Cancer Ther 5: 296-308, 2006.
29. Yang J and Moses MA: Lipocalin 2: A multifaceted modulator of human cancer. Cell Cycle 8: 2347-2352, 2009.

30. Iannetti A, Pacifico F, Acquaviva R, Lavorgna A, Crescenzi E, Vascotto C, Tell G, Salzano AM, Scaloni A, Vuttariello E, *et al*: The neutrophil gelatinase-associated lipocalin (NGAL), a NF-kappaB-regulated gene, is a survival factor for thyroid neoplastic cells. Proc Natl Acad Sci USA 105: 14058-14063, 2008.
31. Tung MC, Hsieh SC, Yang SF, Cheng CW, Tsai RT, Wang SC, Huang MH and Hsieh YH: Knockdown of lipocalin-2 suppresses the growth and invasion of prostate cancer cells. Prostate 73: 1281-1290, 2013.
32. Ruiz-Morales JM, Dorantes-Heredia R, Arrieta O, Chávez-Tapia NC and Motola-Kuba D: Neutrophil gelatinase-associated lipocalin (NGAL) and matrix metalloproteinase-9 (MMP-9) prognostic value in lung adenocarcinoma. Tumour Biol 36: 3601-3610, 2015.
33. Kaur S, Sharma N, Krishn SR, Lakshmanan I, Rachagani S, Baine MJ, Smith LM, Lele SM, Sasson AR, Guha S, *et al*: MUC4-mediated regulation of acute phase protein lipocalin 2 through HER2/AKT/NF-κB signaling in pancreatic cancer. Clin Cancer Res 20: 688-700, 2014.
34. Shiiba M, Saito K, Fushimi K, Ishigami T, Shinozuka K, Nakashima D, Kouzu Y, Koike H, Kasamatsu A, Sakamoto Y, *et al*: Lipocalin-2 is associated with radioresistance in oral cancer and lung cancer cells. Int J Oncol 42: 1197-1204, 2013.
35. Mannelqvist M, Stefansson IM, Wik E, Kusonmano K, Raeder MB, Øyan AM, Kalland KH, Moses MA, Salvesen HB and Akslen LA: Lipocalin 2 expression is associated with aggressive features of endometrial cancer. BMC Cancer 12: 169, 2012.
36. Bolignano D, Donato V, Lacquaniti A, Fazio MR, Bono C, Coppolino G and Buemi M: Neutrophil gelatinase-associated lipocalin (NGAL) in human neoplasias: A new protein enters the scene. Cancer Lett 288: 10-16, 2010.
37. Shrivastava S, Steele R, Sowadski M, Crawford SE, Varvares M and Ray RB: Identification of molecular signature of head and neck cancer stem-like cells. Sci Rep 5: 7819, 2015.